HTML ABSTRACT + LINKS

Ion cyclotron range of frequency mode conversion physics in Alcator C-Mod: Experimental measurements and modeling[a)]

S. J. Wukitch,[b)] Y. Lin, A. Parisot, J. C. Wright, P. T. Bonoli, M. Porkolab, N. Basse, E. Edlund, A. Hubbard, L. Lin, A. Lynn,[c)] E. Marmar, D. Mossessian, P. Phillips,[c)] and G. Schilling[d)]
MIT Plasma Science and Fusion Center, Cambridge, Massachusetts 02139

(Received 19 November 2004; accepted 6 January 2005; published online 7 April 2005)

In ion cyclotron range of frequency experiments, we have simultaneously measured the incident fast wave and the mode converted waves in the mode conversion region in $D(^3He)$ plasmas using an upgraded phase contrast imaging diagnostic in the Alcator C-Mod tokamak [I. H. Hutchinson, R. Boivin, F. Bombarida *et al.*, Phys. Plasmas **1**, 1511 (1994)]. To experimentally validate the full wave TORIC [M. Brambilla, Nucl. Fusion **38**, 1805 (1998)] physics kernel, the simulated power deposition and line integrated perturbed density profiles were compared with experimental profiles and are found to be in remarkably good agreement with the experimentally determined profiles. This suggests the physics model and computation algorithm used in TORIC, particularly for the mode converted waves, model the mode conversion physics well. We also report results from initial mode conversion current drive experiments where the modification of the sawtooth period was clearly observed and was shown to depend on antenna phasing suggesting the presence of a localized driven current. © *2005 American Institute of Physics*. [DOI: 10.1063/1.1866142]

I. INTRODUCTION

In multi-ion species plasmas, one possible absorption mechanism for ion cyclotron range of frequencies (ICRF) waves is mode conversion from the long wavelength fast wave (FW) to short wavelength modes, the ion Bernstein waves (IBW), and ion cyclotron waves (ICW) at the ion-ion hybrid resonance.[1–3] This process can also be found in space physics where energetic ions are thought to be generated through interaction with mode converted ICW waves in the earth's ionosphere.[4] Mode conversion is of interest for magnetic fusion due to its localized nature and possible control applications. Mode converted waves are strongly damped in the vicinity of the mode conversion surface via electron Landau damping and can be damped by ions at the Doppler broadened ion cyclotron resonance. Localized plasma heating has been investigated on a number of devices including tokamak at Fontenay aux Roses,[5] Tokamak Fusion Test Reactor (TRTF),[6,7] Tore Supra,[8,9] Joint European Torus,[10] Axially Symmetric Diverted Experiment Upgrade,[11,12] and Alcator C-Mod (Refs. 13–18) for various scenarios. Mode conversion current[6,7] and flow drive[19] results have been reported and are potentially important tools to control the local plasma current profile for suppression of sawteeth and neoclassical tearing modes and to suppress plasma turbulence in advanced tokamak plasma regimes. Another potential application using mode converted IBW is to localize lower hybrid wave absorption off axis and has been recently demonstrated via direct launched IBW.[20] Details of mode converted wave propagation and absorption can affect the efficiency of the desired response.

An important element for any physics code development is to experimentally validate the underlying physics models through comparisons of the simulations with experimental measurements. Through discharge analysis, the underlying physics models and computational algorithms can be tested. Experimental verification of code predictions is essential for reliable predictive capability in future burning plasma experiments (ITER). In the ICRF mode conversion scenario, the simulations need to resolve multiple wavelength waves from 0.1 cm to 10 cm. A number of codes are available to simulate ICRF mode conversion experiments including TORIC (full wave, finite Larmor radius code),[21–23] ALCYON coupled with RAYS,[24] and AORSA2D (full wave, all orders code).[25] As with previous C-Mod discharge analysis, TORIC is used to simulate the experimental results described below.

The fast wave dispersion relation in cold, homogeneous plasma can be written as[3]

$$n_\perp^2 = (n_\parallel^2 - R)(n_\parallel^2 - L)/(S - n_\parallel^2),$$

where $n_\parallel$ and $n_\perp$ are the parallel and perpendicular index of refraction and the parameters R, L, and S are the usual Stix definitions.[1] The vanishing numerators correspond to the right ($R=n_\parallel^2$) and left ($L=n_\parallel^2$) hand cutoff layers and the mode conversion location is indicated by the vanishing of the denominator, or ion-ion hybrid resonance location, $S=n_\parallel^2$. At the mode conversion location, hot plasma corrections become important and the FW can couple to the IBW while sheared B-field allows coupling to the ICW. An example of the full dispersion relation is shown in Fig. 1 where the FW and IBW dispersion is calculated along the midplane and the

[a)]Paper RI1 2, Bull. Am. Phys. Soc. 49, 324 (2004).
[b)]Invited speaker.
[c)]Also at UT Fusion Research Center, Austin, TX.
[d)]Also at Princeton Plasma Physics Laboratory, Princeton, NJ.

 © 2005 American Institute of Physics

Downloaded 11 Apr 2005 to 198.125.178.190. Redistribution subject to AIP license or copyright, see http://pop.aip.org/pop/copyright.jsp

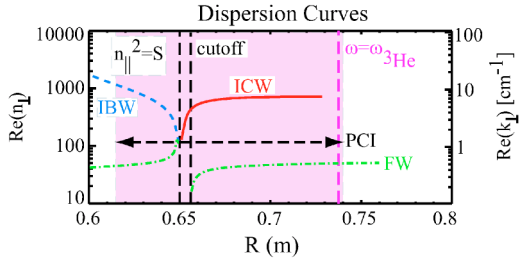

FIG. 1. Dispersion relation in a $D(^3\mathrm{He})$ plasma where the FW and IBW branch are calculated along the midplane and the ICW dispersion is calculated for a flux surface tangent to the mode conversion surface at $r=3$ cm in the lower half plane (PCI chord location is also shown).

ICW dispersion is calculated for a flux surface tangent to the mode conversion surface at $r=3$ cm in the lower half plane (the ICW propagates roughly along the B flux surface).[26] The wavelengths of the FW, ICW, and IBW are ≈10 cm, 1–2 cm, and 0.3 cm, respectively. As originally shown in Ref. 2, the poloidal B field B_θ plays a crucial role in coupling the FW to the ICW which is restricted to the edge plasma without magnetic shear. High poloidal mode numbers in the mode converted wave fields are converted to large parallel wave numbers via the magnetic shear. Both TORIC and AORSA2D numerical simulations indicate the sheared B field strongly influences whether mode conversion to IBW or ICW is dominant.[18,23,27] As shown in Fig. 2 for a H–^{3}He–D discharge, the IBW propagates to the high field side of the mode conversion surface while the ICW propagates to the low field side above and below the midplane. In addition, the mode converted wave fields are up-down asymmetric. The ICW propagates roughly along a flux surface and back towards the antenna. By definition, the poloidal angle θ is defined to be 0 at the outboard midplane and increases in the counterclockwise direction and the poloidal wave number k_θ for ICW waves propagating counterclockwise is positive. Therefore, waves with positive toroidal mode numbers N_ϕ propagating below the midplane up-shift immediately and are rapidly damped. For $N_\phi > 0$, the parallel wave number, $k_\parallel \cong k_\theta + k_\phi = (m/r)(B_\theta/B) + [(N_\phi/R)(B_\phi/B)]$ (m is poloidal mode number, r is minor radius, B is the total magnetic field, R is major radius, and B_ϕ is toroidal magnetic field), reverses sign in the upper half plane and waves propagate further before damping. The first experimental indication of ICW in the plasma core were from phase contrast imaging (PCI) measurements of the mode conversion region for ^{3}He–D–H plasmas with an ion mix of 23% ^{3}He, 21% D, 33% H.[16] The measured wave number and the spatial fluctuation profile relative to the mode conversion layer were in agreement with the numerical simulations.

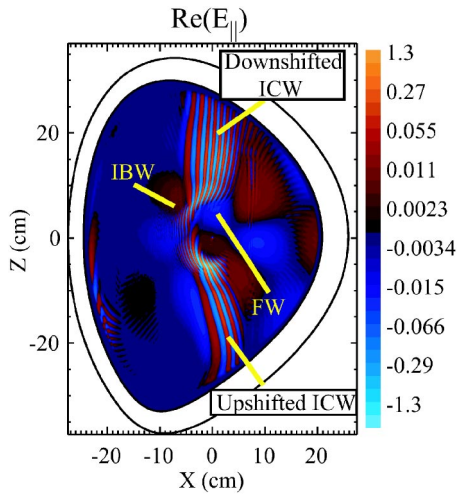

FIG. 2. Parallel electric field contours from a TORIC simulation for a H–^{3}He–D discharge showing the incoming fast and mode converted waves.

To verify mode conversion physics, a complete experimental measurement and simulation comparison of the measured mode converted waves and the plasma response is important. This requires measuring waves of various wavelengths over a wide region of plasma. Compared with previously reported work, the diagnostic coverage for these experiments is significantly improved. The PCI has been upgraded to 32 channels allowing the observation of a large region of the radial plasma cross section and a wide range of wave numbers simultaneously, although without information on vertical localization along the laser beam. As described below, the power deposition profile resolution has been increased from nine channels to 32 channels for the ~5 T discharges. In this paper we shall summarize both experimental observations and code predictions of ICRF mode conversion. We also present here initial results from current drive experiments on C-Mod and current drive predictions for a model discharge. The remainder of the paper is organized as follows: Sec. II contains the experimental setup and TORIC description, Sec. III discusses the data and simulation comparison, Sec. IV discusses the initial mode conversion current drive results, and Sec. V concludes this paper.

II. EXPERIMENTAL SETUP AND TORIC DESCRIPTION

Alcator C-Mod is a compact (major radius $R=0.67$ m, minor radius $a=0.22$ m), high field ($B_T \leqslant 8.1$ T) diverted tokamak.[28] The discharges analyzed here are single null L-mode $D(^3\mathrm{He})$ minority (minority in parentheses) ICRF heated discharges. The on-axis toroidal fields B_T were 5.1–5.6 T and 8 T, and the plasma current I_p was 0.8–1 MA with the central density $\leqslant 2\times10^{20}$ m^{-3}. The ICRF heating power is coupled to the plasma via three fast wave antennas, see Fig. 3. The two-strap antennas, D and E,[29] are operated in the heating mode $(0,\pi)$ phasing at 80 MHz and the four-strap antenna J (Ref. 30) is operated at 50 MHz for the 5 T discharges and 78 MHz for the 8 T discharges. This places the ^{3}He cyclotron resonance on the low field side of the magnetic axis for the 5 T discharges and near axis for the 8 T discharges. The J antenna injected up to 1.5 MW for both heating $(0,\pi,\pi,0)$ and co-current and counter current drive $(0,\pm\pi/2,\pm\pi,\pm3\pi/2)$ phasing. For the ~5 T D(H) discharges, at 80 MHz the H minority cyclotron resonance is located near the magnetic axis.

The primary plasma diagnostics in this study are the following: a grating polychromator (GPC) (Ref. 31) and second harmonic heterodyne (FRCECE) electron cyclotron emission

Downloaded 11 Apr 2005 to 198.125.178.190. Redistribution subject to AIP license or copyright, see http://pop.aip.org/pop/copyright.jsp

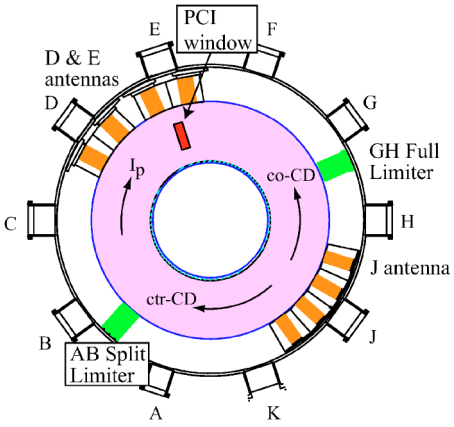

FIG. 3. Top view of the C-Mod tokamak showing the location of the three antennas and the position of the wave diagnostic location. The direction of wave launch is also shown for co-current and counter current drive antenna phasing.

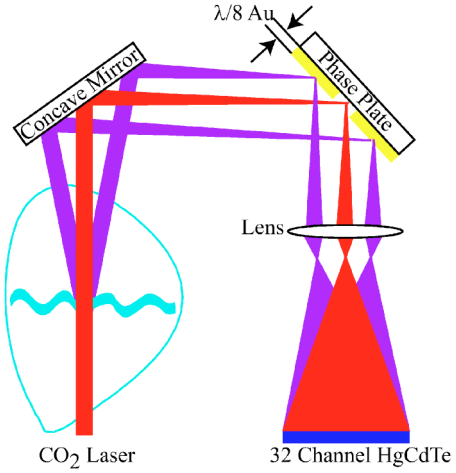

FIG. 4. C-Mod poloidal cross section showing the location of the PCI cords and ECE diagnostics.

diagnostics[32] measure electron temperature and Thomson scattering measures plasma density.[33,34] The GPC is a nine channel system with ~1 cm resolution (spacing is ≈2–3 cm between channels) and temporal resolution of 50 μs and is the primary electron temperature measurement at 8 T. For ~5 T discharges, the 32 channel FRECE diagnostic is used to provide high spatial (~0.7 cm) and temporal (10 μs) resolution profile measurements. A core and edge Thomson scattering system records the electron temperature and density profiles. The diagnostic positions are mapped to the plasma midplane or flux surface position via EFIT.[35] The H to D ratio is monitored by the ratio of H_α to D_α in the plasma edge.[36]

The electron power deposition profile is determined by examining the "break in slope" of the stored electron kinetic energy.[37] Assuming the changes in radiated power, Ohmic heating, and transport are negligible compared to the local rf heating rate, the local absorbed power is

$$S_{abs} \approx \frac{3}{2} n_e \Delta \left\{ \frac{\partial T_e}{\partial t} \right\},$$

where the time window to calculate the slope preceding and post rf transition is taken to be 0.5–1.0 ms for the data presented here. For the data presented here, several fast rf transitions occurred within ~0.1 s allowing for multiple transitions, typically 5, to be analyzed and averaged. The error bars reflect one standard deviation.

The primary rf wave diagnostic is a CO_2 laser based PCI diagnostic.[38,39] The PCI diagnostic converts phase variation arising from density fluctuations to intensity variation through the interference of the scattered and $\lambda/4$ phase-shifted unscattered beam passing through the plasma. The beam is imaged onto a 32 channel HgCdTe photoconductive detector. The detector output is digitized at 10 MHz and the system has a frequency range of $2\ \text{kHz} < f < 5\ \text{MHz}$. The beam, typically expanded to 12 cm in the experiments described here, makes a vertical pass through the plasma as shown in Fig. 4. For the current C-Mod PCI diagnostic, the minimum wave number is determined by the beam width and is typically 0.4–0.5 cm^{-1} for the experiments described herein. The maximum wave number is determined by the channel separation, controlled by the magnification of the image onto the detector, and is typically 8 cm^{-1} for the present experiments. The PCI is most sensitive to waves propagating perpendicular to the beam path; therefore, the diagnostic is most sensitive to waves with significant wave number along the major radius k_R.

To detect density fluctuations associated with the rf mode converted waves at 50 and 78 MHz, the laser intensity is modulated near the rf frequency. The selected modulation frequency is shifted from the rf frequency typically ≤1 MHz, for example, 50.75 MHz. When the 50 MHz fluctuation in the plasma is illuminated by the 50.75 MHz modulated laser, the image intensity (which is the product of both) reveals a 750 kHz beat oscillation, the frequency at which the signal is detected. The PCI diagnostic is calibrated before each discharge with a sound wave at 15 kHz passing across the laser beam. This is then utilized to determine the PCI chord positions and the relative channel to channel calibration at 15 kHz. This relative calibration is assumed to be frequency independent up to 5 MHz. In principle, an absolute calibration is possible if the sound burst and the laser power are accurately characterized (necessary for comparing the absolute experimental and theoretical values).

The principal simulation tool is the ion finite Larmor radius (FLR) full wave code TORIC. The code has been described in detail in a number of references[21–23] and will be described here briefly. For a fixed frequency and N_ϕ, TORIC solves Maxwell's equations for an axisymmetric toroidal plasma, including an antenna model, assuming a linear response using a mixed spectral-finite element basis. Utilizing a FLR expansion (Swanson–Colestock–Kashuba approximation), the plasma current response retains terms up to second harmonic in the ion cyclotron frequency. If treated in this fashion, the electron Landau damping (ELD) for the IBW is strongly suppressed.[21] Thus, a correction is required to the FLR expansion to properly account for the ELD of the IBW or ICW. The ELD predicted by the local dispersion relation can be simulated by adding an imaginary part $\delta\sigma$ to the FLR

Downloaded 11 Apr 2005 to 198.125.178.190. Redistribution subject to AIP license or copyright, see http://pop.aip.org/pop/copyright.jsp

coefficient σ, where the imaginary part is calculated from the local dispersion relation retaining all orders in $k_\perp \rho_i$. This approach has the advantage of simulating the ELD predicted by the local dispersion relation without altering the structure of the equations, modifying the damping of the FW, or changing the mode conversion efficiency. In addition, this approach lends itself to efficient numerical calculation resulting from the sparse block tridiagonal nature of its stiffness matrix. Although the simulation approach for calculating IBW ELD is somewhat heuristic, TORIC has been compared with METS (Ref. 40) [a one-dimensional (1D) all orders code] and found to have good agreement in the power absorption on electrons and ions.[15] TORIC has also been compared with AORSA2D and found to have qualitative agreement of the 2D E fields in mode conversion scenarios where $k_\perp \rho_i \leqslant 1$.[23] This suggests the less computationally intensive TORIC model could possibly simulate mode conversion scenarios for C-Mod. As a result of the poloidal mode coupling in a tokamak, a large number of poloidal modes m are required to represent discontinuities such as mode conversion. For the current TORIC basis, the resolution requirements can be estimated from the condition that $k_\perp \rho_i \sim 1$ and $k_\perp \sim m/r$.[15] For the C-Mod experiments discussed here, $m \leqslant 255$ modes are sufficient for converged solutions. In order to routinely carry out large poloidal mode simulations, TORIC has been parallelized[23] and further improvements in the code algorithm have allowed for 255 mode simulations to become routine on an "in-house" 48 processor computer cluster "Marshall".[23] Using all 24 nodes, a 255 poloidal mode run for a single N_ϕ requires $\approx$30 min of wall clock time to compute. Thus, discharge analysis for mode conversion scenarios with the entire antenna spectrum included is not prohibitive. To calculate the local absorbed power (and similarly for the perturbed density fluctuation), the total absorbed power is the sum over the launched spectrum, typically $-20 < N_\phi < 20$, weighted by the vacuum spectrum $G(N_\phi)$ and the relative coupling resistance,

$$S_{abs}^{TORIC} = \sum_{N_\phi} G(N_\phi) \frac{R_L(N_\phi)}{\sum R_L(N_\phi)} P_{abs}^{TORIC}(N_\phi),$$

where $R_I(N_\phi)$ is the coupling resistance calculated by TORIC and $P_{abs}(N_\phi)$ is the calculated local absorbed power. To enable discharge analysis, TORIC has been modified to accept EFIT calculated magnetic geometry. This is an important advancement in discharge analysis because 2% changes in the total magnetic field can result in 1–2 cm shifts of the mode conversion layer in the plasma core.

The TORIC antenna model is somewhat simplified over a 3D antenna structure and includes a Faraday screen, a scrape off layer, and the vacuum chamber wall. The scrape off layer (SOL) starts at the last closed flux surface (LCFS) and vacuum is assumed outside the LCFS. In the experiment, the SOL extends from the LCFS to the vacuum vessel wall and in C-Mod the FW cutoff is located at the plasma limiter, typically 1 cm outside the LCFS. Therefore, the antenna is modeled by moving it to a position such that the distance to cutoff is the same as in the experiment and the vacuum spectrum is evaluated at the real antenna position. This simplification thus ignores the effects of edge density gradients and density pedestal height on the loading resistance[41] which could be particularly important for H-mode discharge analysis.

To analyze the density fluctuations measured by the PCI, a synthetic diagnostic has been added to the TORIC postprocessing. The density fluctuations associated with the rf waves are proportional to the divergence of the perturbed electron velocity v_{e1}, and it can be related to the rf electric fields through the linearized electron fluid force balance equation[42]

$$\frac{\tilde{n}_e}{n_{e0}} = \frac{-i}{\omega} \nabla \cdot \mathbf{v}_{e1},$$

$$\mathbf{v}_{e1} \cong -i \frac{\Omega_e}{\omega} \frac{E_\zeta}{B_0} \hat{\zeta} + \frac{E_\eta}{B_0} \hat{\psi} - \frac{E_\psi}{B_0} \hat{\eta},$$

where Ω_e is electron cyclotron frequency, ω is the rf frequency, ζ is coordinate along the B field, η and Ψ are perpendicular to the B-field line, $\Omega_e/\omega \gg 1$, and $E_\eta \sim E_\psi$. This suggests the density fluctuations will be most intense where the product of the wave number and field intensity is largest. Using the rf electric fields from TORIC, the 2D density fluctuations associated with the rf waves can be calculated. These fluctuations are convolved with PCI instrumental sensitivity and geometry to produce the expected line integrated density fluctuation profile.

To evaluate mode conversion and fast wave current drive scenarios in C-Mod, TORIC is coupled to a current drive package based upon Ehst and Karney parametrization of the current drive efficiency:[43]

$$J_{RF}(\psi) = \int_0^{2\pi} d\theta \sum_m G_{RF}^m(\psi, \theta_i) \sum_{m'} P_{abs}^{m,m'}(\psi, \theta_i),$$

$$G_{RF}^m(\psi, \theta_i) = G_{RF}(v_{||} = \omega/k_{||}, \varepsilon = r/R),$$

where ψ is the poloidal flux coordinate, θ_i is the poloidal angle, $G_{RF}^m(\psi, \theta_i)$ is a parametrization of the current drive efficiency computed from an adjoint solution to Fokker Planck equation, and $P_{\mathrm{abs}}^{\mathrm{m,m}}$ is the calculated local absorbed power for a given N_ϕ from TORIC. This formulation directly includes particle trapping by convolving the local power absorbed with the current drive efficiency at that position. Furthermore, the variation of the parallel wave number is directly accounted for because the power absorption is reconstructed as a function of the poloidal mode number. This will be critically important for both the IBW and ICW where the poloidal component of the parallel wave number can dominate the toroidal contribution.

III. EXPERIMENTAL ANALYSIS AND SIMULATIONS

Using J antenna at 50 MHz, $D(^3\mathrm{He})$ plasmas were investigated to simultaneously measure the waves in the mode conversion region. A series of L-mode discharges were performed at $B_T = 5.2$, 5.4, and 5.6 T at $\sim$25% ^{3}He concentration, thereby moving the mode conversion layer from the high field side of the magnetic axis to the low field side (LFS). The dispersion relation is plotted for a representative,

Downloaded 11 Apr 2005 to 198.125.178.190. Redistribution subject to AIP license or copyright, see http://pop.aip.org/pop/copyright.jsp

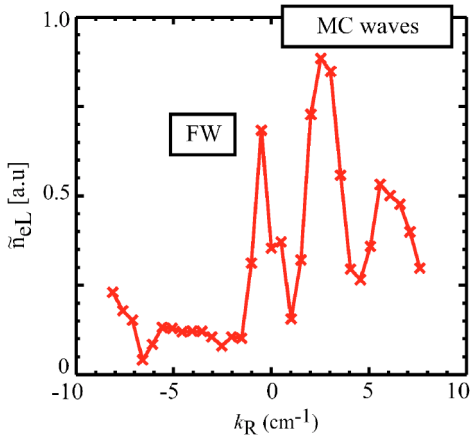

FIG. 5. Measured wave number spectrum showing both the fast wave and mode converted waves in the mode conversion region.

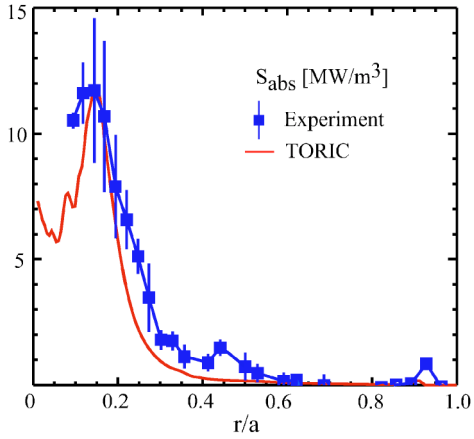

FIG. 7. Comparison of the calculated and measured power deposition profile for $D(^3\mathrm{He})$, 5.6 T discharge.

5.3 T discharge with 20% ^{3}He minority in Fig. 1. Compared to earlier work, the mode conversion region is within the PCI coverage and a representative measured wave number spectrum is shown in Fig. 5 for a 5.4 T discharge. As a result of differences in wavelength, the low k_R are likely to be the forward and reflected FW and two peaks from the mode converted waves. The multiple peaks could result from the up-down asymmetry associated with the mode converted waves. Caution should be used in identifying particular waves from this data because of the line integrated nature of the PCI data and the presence of multiple waves in the plasma cross section. This is the first instance where the mode converted waves and the FW have been measured simultaneously in the mode conversion region. For a series of discharges where the B field is increased from 5.1 to 5.6 T, the line integrated fluctuation data at the heterodyne frequency, $\tilde{n}_{eL}=\int\tilde{n}_e dl$, are shown in Fig. 6. Note that in agreement with expectations, the maximum $\tilde{n}_{eL}$ moves towards the LFS as B_T increases.

Since simple interpretation of the local k is difficult because of the multiple waves present and geometrical effects, the experimental data are compared with a synthetic PCI diagnostic (simulated diagnostic response as calculated from TORIC). To determine the ^{3}He fraction, the ^{3}He fraction is set in the simulation by matching the location of the peak in the power deposition profile (no restriction is placed upon the magnitude). The calculated deposition agrees well with the experiment and is shown in Fig. 7. The synthetic PCI data is then compared with the experimental data and the comparison for the 5.6 T is shown in Fig. 8. The agreement between the simulation and the experiment is excellent with respect to the profile shape. Recalling that the IBW is found to propagate on the high field side of the mode conversion layer and the ICW on the low field side, the feature near the high field side of the mode conversion layer is the IBW and the fluctuation on the low field side is the ICW. This is the first instance where the power deposition profile (plasma response) and the associated waves have been simultaneously measured for ICRF mode conversion. The good agreement between simulation and experiment suggests the physics model and computational algorithm used in TORIC, particularly for the mode converted waves, model the data well.

Future experiments using a masking technique[44] to obtain localization along the cord could allow direct confirmation of the mode converted wave up-down asymmetry and allow further testing of the TORIC physics model. Further tests of the relative density fluctuation amplitude of the mode converted waves can be tested by varying the antenna phasing. An interesting observation obtained from the TORIC simulations is the strong dependence of the relative strength of the mode converted waves on the antenna spectrum.

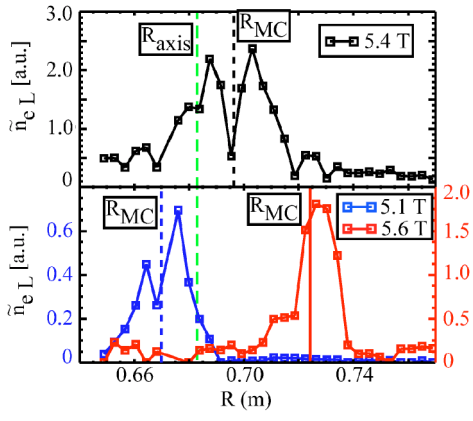

FIG. 6. Line integrated fluctuation data at the heterodyne frequency showing the spatial profile shifts to larger major radius as the field is increased from 5.1 T to 5.6 T.

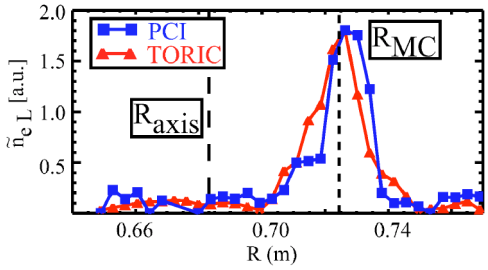

FIG. 8. Comparison of experimental (blue) and synthetic (red) line integrated density fluctuations demonstrating remarkably good agreement.

Downloaded 11 Apr 2005 to 198.125.178.190. Redistribution subject to AIP license or copyright, see http://pop.aip.org/pop/copyright.jsp

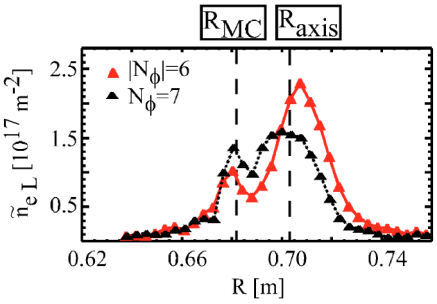

FIG. 9. The relative contribution of ICW and IBW to the fluctuation profile is predicted to be sensitive to the antenna vacuum spectrum as shown by comparison of TORIC simulation of two vacuum spectrums peaked at $N_\phi=6$ (red) and $N_\phi=7$ (dashed black).

Shown in Fig. 9 is a comparison of two profiles calculated with a vacuum spectrum symmetric about zero and peaked at $|N_\phi|=6$ and a vacuum spectrum asymmetric about zero and peaked at $N_\phi=7$. The relative strength of the IBW to ICW has changed dramatically and the width of the ICW profile is much broader for the $|N_\phi|=6$ than the $N_\phi=7$. Upgrades to the diagnostic's high k_R resolution may allow direct monitoring of the wave number up shift. Finally, a comparison of the absolute magnitudes of the fluctuation level is left for future work.

IV. MODE CONVERSION CURRENT DRIVE

Due to the localized nature of the power deposition, mode conversion current drive (MCCD) has the potential to provide local current profile control. For example, as noted in Ref. 45 the rapid up shift of $k_\parallel$ of the IBW can, in principle, result in the degradation of wave directionality because of poloidal up-down asymmetry, thus leading to a loss of net current drive efficiency. In the case of current drive by ICW, mode conversion efficiency should be maximized, and particle trapping should be minimized to optimize off-axis current drive efficiency.

The first experimental investigation of MCCD was performed in TFTR.[6,7] Here the driven current was estimated from a change in loop voltage. The goal of the experiments described below was to experimentally determine the optimum species mix for efficient mode conversion and have the wave in the PCI viewing region. These experiments utilized the *J* antenna at 78 MHz in *D* plasmas with a ^{3}He minority. For central deposition, $B_T=8$ T, $I_p=0.8$ MA, and the minority was scanned to maximize the electron deposition. The *D* antenna operated in heating phase was at 1 MW power level and the *J* antenna was typically at 1.5 MW. In principle, the driven current could be deduced from the change in the loop voltage for co-current and counter current drive phasing. However, the constraints of the experiment resulted in a situation where the fraction of mode converted power was measured to be ~30% of the total injected power or 0.3 MW, determined by integrating the measured power deposition profile. From TORIC simulations, the expected net driven current was ~10 kA, too small to result in significant change in loop voltage, but the peak driven current density was of the order of local Ohmic current density. As previously

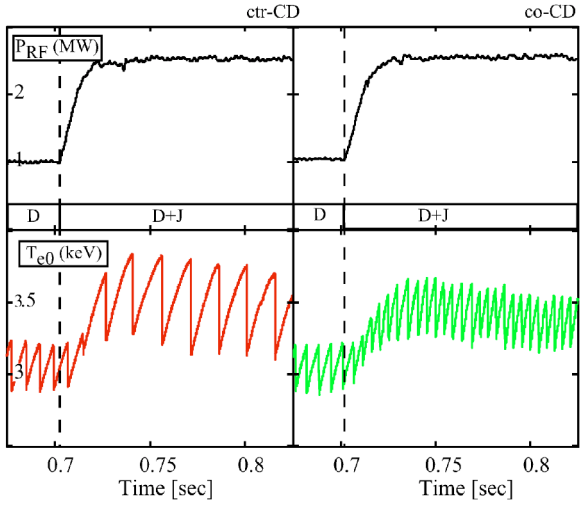

FIG. 10. Top panels show the rf power traces for the two discharges where the antenna phase was changed from counter-CD to co-CD phasing. The sawtooth period is lengthened for the ctr-CD case (left panel) and shortened for the co-CD case (right panel) consistent with increasing the sawtooth period by lowering the shear at the $q=1$ surface.

demonstrated,[46,47] the sawtooth oscillation can provide a means to infer the presence of a local change in the current profile. The sawtooth period can be lengthened (shortened) by decreasing (increasing) the current gradient at the $q=1$ surface. As shown in Fig. 10, the sawtooth period lengthens to 15 ms for counter current drive phasing and shortens to 5 ms for co-current drive phasing. From the measured power deposition profiles shown in Fig. 11, the deposition profiles for co-current and counter current drive phasing are similar and the peak of the deposition is just inside the $q=1$ radius. Furthermore, comparing two counter current drive phasing discharges where the deposition is moved from near the $q=1$ surface to near the axis finds that the near axis deposition does not significantly modify the sawtooth period, see Figs. 12 and 13. This is consistent with a localized driven current near the mode conversion surface. Further experiments could better demonstrate that the change in sawtooth period is a result of locally driven current by sweeping the mode con-

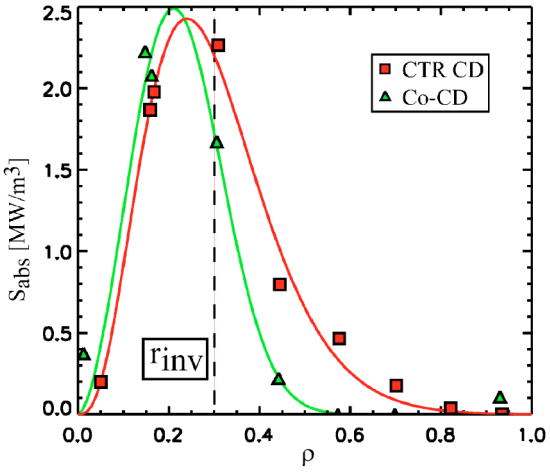

FIG. 11. The co-current and counter current drive power deposition profiles from single rf transition off are similar.

Downloaded 11 Apr 2005 to 198.125.178.190. Redistribution subject to AIP license or copyright, see http://pop.aip.org/pop/copyright.jsp

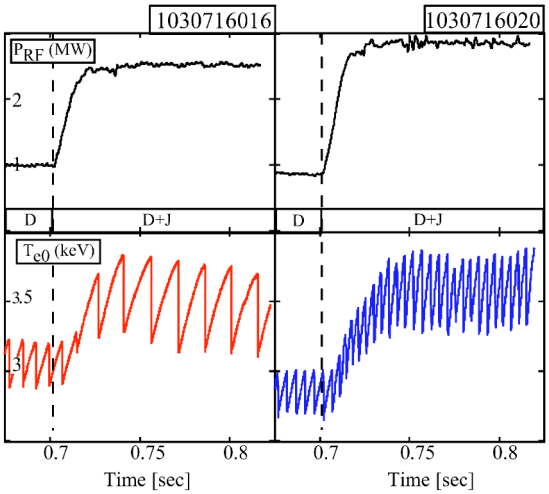

FIG. 12. Top panels show the rf power traces for the two discharges where the antenna phase was changed from ctr-CD with different B_T. For the power deposition peaked near the $q=1$ surface (left panel), the sawtooth period increases and is unchanged when the deposition is inside the $q=1$ surface.

version surface for a given antenna phasing from just inside to just outside the $q=1$ surface. For counter-CD phasing, deposition just outside the $q=1$ should result in shortened sawteeth (current gradient is increased) and deposition just inside the $q=1$ should result in longer sawteeth (current gradient is decreased).

Using TORIC, simulations have been used to investigate the optimum parameters required to maximize the net driven current and characterize the influence of wave propagation on the driven current (see Fig. 14). A model discharge was identified with $B_T=5.4$ T, $n_{e0}=1\times10^{20}$ m^{-3}, and $T_{e0}=5$ keV. Although on the low end of the normal C-Mod density range, this type of discharge has been achieved. The species mix used in the analysis is D: 65%, ^{3}He: 15%, and H: 5%. The simulation shows ~100 kA can be driven for 3 MW ICRF power injected corresponding to an efficiency, $\eta=(IRn)/P$ (where I is the driven current, R is major radius, n is the plasma density, and P the injected power), of 0.022 A/W m^2. This calculated efficiency is in reasonable agreement with the empirical current drive efficiency scaling

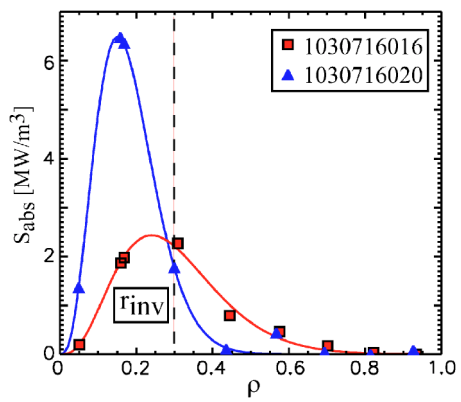

FIG. 13. Measured power deposition profiles for the ctr-CD phasing at 8.1 T and 7.9 T.

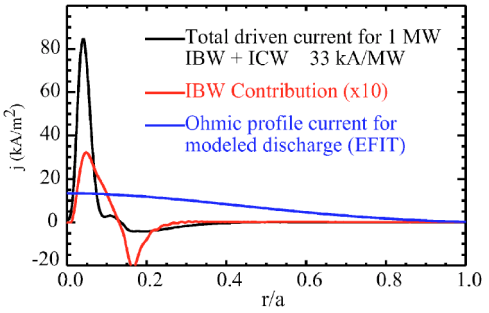

FIG. 14. Predicted current profile for $D(^3\text{He})$ mode conversion scenario based upon $T_{e0}=5$ keV and $n_{e0}=1\times10^{20}$.

found for fast wave current drive that have $v_\phi/v_{te}\sim1$ (where v_ϕ is the wave phase velocity and v_{te} is the electron thermal velocity).[3] The simulations show that the driven current by mode converted IBW has a bipolar nature suggesting this branch should be minimized to maximize the net driven current. The ICW contribution also has a small off-axis reversal resulting from the up-down asymmetry in the ICW wave propagation. This result suggests that maximum driven current condition is where the ICW branch dominates and is strongly absorbed by electron Landau damping.

V. CONCLUSIONS

We have reported experimental results where the mode converted waves and incident fast wave are simultaneously measured in the mode conversion region in $D(^3\text{He})$ plasmas during ICRF experiments in the Alcator C-Mod tokamak. In addition, the TORIC simulated power deposition and line integrated perturbed density profile are found to be in remarkably good agreement with the experimentally determined profiles. Therefore the physics assumptions and computational algorithm used in TORIC, particularly for the mode converted waves, model the mode conversion physics well. A novel feature of this work is that the waves responsible for localized electron heating have been monitored by a phase contrast imaging diagnostic in the high temperature and high density plasma core. Exploiting the localized nature of mode conversion, initial experiments on mode conversion current drive where small net current is predicted near the $q=1$ surface were performed using the sawtooth period as an indicator of driven current. The modification of the sawtooth period was clearly observed and was shown to depend on antenna phasing suggesting the presence of a localized driven current.

ACKNOWLEDGMENTS

The authors thank the Alcator C-Mod team for their contributions to these experiments, specifically Charley Schwartz (RF engineer) who has since died in a private airplane accident. This research utilized the MIT Plasma Science and Fusion Center Theory Group parallel computational cluster. This work was supported by the Department of Energy.

Downloaded 11 Apr 2005 to 198.125.178.190. Redistribution subject to AIP license or copyright, see http://pop.aip.org/pop/copyright.jsp

[1]T. H. Stix, *Waves in Plasmas* (American Institute of Physics, New York, 1992).
[2]F. W. Perkins, Nucl. Fusion **17**, 1197 (1977).
[3]M. Porkolab, A. Becoulet, P. T. Bonoli *et al.*, Plasma Phys. Controlled Fusion **40**, A35 (1998).
[4]T. Chust and D. Le Queau, J. Geophys. Res. **101**, 10695 (1996); **98**, 13 (1993); **98**, 363 (1993).
[5]T. F. R. Equipe, *Plasma Physics and Controlled Nuclear Fusion Research*, Proceedings of the ninth Conference on Plasma Physics and Controlled Nuclear Fusion, Baltimore, 1982 (IAEA, Vienna, 1983), Vol. 2, p. 17.
[6]R. Majeski, J. H. Rogers, S. H. Batha *et al.*, Phys. Plasmas **3**, 2006 (1996).
[7]R. Majeski, J. H. Rogers, S. H. Batha *et al.*, Phys. Rev. Lett. **76**, 764 (1996).
[8]S. Saoutic, A. Bécoulet, T. Hutter, D. Fraboulet, A. K. Ram, and A. Bers, Phys. Rev. Lett. **76**, 1647 (1996).
[9]I. Monakhov, V. Basiuk, A. Bécoulet, F. Imbeaux, F. Nguyen, Yu. Petrov, and Y. Peysson, *Europhysics Conference Abstracts, 26th EPS Conference on Controlled Fusion and Plasma Physics, Maastricht, 1999* (European Physical Society, 1999), Vol. 23J, p. 81.
[10]M. J. Mantsinen, M.-L. Mayoral, D. Van Eester *et al.*, Nucl. Fusion **44**, 33 (2004).
[11]J.-M. Noterdaeme, S. Wukitch, D. A. Hartmann *et al., Proceedings of the 16th IAEA Fusion Energy Conference* (IAEA, Vienna, 1996), p. IAEA-CN-64/E1-EP-4.
[12]J.-M. Noterdaeme, M. Brambilla, B. Brüsehaber *et al., Europhysics Conference Abstracts, 26th EPS Conference on Controlled Fusion and Plasma Physics, Maastricht, 1999* (European Physical Society, 1999), Vol. 23J, p. 1561.
[13]Y. Takase, R. L. Boivin, F. Bombarda *et al.*, Plasma Phys. Controlled Fusion **38**, 2215 (1996).
[14]Y. Takase, R. L. Boivin, F. Bombarda *et al.*, Phys. Plasmas **4**, 1647 (1997).
[15]P. T. Bonoli, M. Brambilla, E. Nelson-Melby *et al.*, Phys. Plasmas **7**, 1886 (2000).
[16]E. Nelson-Melby, M. Porkolab, P. T. Bonoli *et al.*, Phys. Rev. Lett. **90**, 155004 (2003).
[17]Y. Lin, S. Wukitch, P. T. Bonoli *et al.*, Plasma Phys. Controlled Fusion **45**, 1013 (2003).
[18]Y. Lin, S. Wukitch, P. T. Bonoli *et al.*, Phys. Plasmas **11**, 2466 (2004).
[19]C. K. Phillips, M. G. Bell, R. E. Bell *et al.*, Nucl. Fusion **40**, 461 (2000).
[20]B. Wan, Y. Shi, G. Xu *et al.*, Phys. Plasmas **11**, 2543 (2004).
[21]M. Brambilla, Nucl. Fusion **38**, 1805 (1998).
[22]M. Brambilla, Plasma Phys. Controlled Fusion **41**, 1 (1999).
[23]J. C. Wright, P. T. Bonoli, M. Brambilla *et al.*, Phys. Plasmas **11**, 2473 (2004).
[24]Yu. Petrov, A. Becoulet, and I. Monakhov, Phys. Plasmas **7**, 911 (2000).
[25]E. F. Jaeger, L. A. Berry, E. D'Azevedo, D. B. Batchelor, M. D. Carter, and K. F. White, and H. Weitzner, Phys. Plasmas **9**, 1873 (2002).
[26]F. W. Faulconer, D. Van Eester, and R. R. Weynants, *14th European Conference on Controlled Fusion and Plasma Physics* (European Physical Society, Petit-Lancy, 1987),Vol. 11D, p. 932.
[27]E. F. Jaeger, L. A. Berry, J. R. Myra *et al.*, Phys. Rev. Lett. **90**, 195001 (2003).
[28]I. H. Hutchinson, R. Boivin, F. Bombarda *et al.*, Phys. Plasmas **1**, 1511 (1994).
[29]Y. Takase, S. N. Golovato, M. Porkolab, K. Bajwa, H. Becker, and D. Caldwell, *14th Symposium on Fusion Engineering, San Diego, 1992* (IEEE, Piscataway, NJ, 1992), p. 118.
[30]S. J. Wukitch, R. L. Boivin, P. T. Bonoli *et al.*, Plasma Phys. Controlled Fusion **46**, 1479 (2004).
[31]P. J. O'Shea and A. E. Hubbard, *Proceedings of the Ninth Joint Workshop on Electron Cyclotron Emission and Electron Cyclotron Heating, Borrego Springs, CA* (World Scientific, Singapore 1995) p. 393.
[32]J. W. Heard, C. Watts, R. F. Gandy, P. E. Phillips, G. Cima, R. Chatterjee, A. Blair, A. Hubbard, C. W. Domier, and N. C. Luhmann, Jr., Rev. Sci. Instrum. **70**, 1011 (1999).
[33]J. W. Hughes, D. A. Mossessian, A. E. Hubbard, E. S. Marmar, D. Johnson, and D. Simon, Rev. Sci. Instrum. **72**, 1107 (2001).
[34]J. W. Hughes, D. A. Mossessian, K. Zhurovich, M. Demaria, K. Jensen, and A. E. Hubbard, Rev. Sci. Instrum. **74**, 1667 (2003).
[35]L. L. Lao, H. St. John, R. D. Stambaugh, A. G. Kellman, and W. Pfeiffer, Nucl. Fusion **25**, 1611 (1985).
[36]T. E. Tutt, Master's thesis, Massachusetts Institute of Technology, 1999.
[37]D. J. Gambier, M. P. Evrard, J. Adam *et al.*, Nucl. Fusion **30**, 23 (1990).
[38]S. Coda and M. Porkolab, Rev. Sci. Instrum. **66**, 454 (1995).
[39]A. Mazurenko, Ph. D. thesis, Massachusetts Institute of Technology, 2001.
[40]D. N. Smithe *et al., 12th Top. Conference on Radio Frequency Power in Plasmas, Savannah, GA*, edited by P. Ryan and T. Intrator (American Institute of Physics, New York, 1997) Vol. 403, p. 367.
[41]A. Parisot, S. J. Wukitch, P. T. Bonoli, J. W. Hughes, B. LaBombard, Y. Lin, R. Parker, M. Porkolab, and A. K. Ram, Plasma Phys. Controlled Fusion **46**, 1781 (2004).
[42]E. Nelson-Melby, Ph.d. thesis, Massachusetts Institute of Technology, 2001.
[43]D. A. Ehst and C. F. Karney, Nucl. Fusion **31**, 1933 (1991).
[44]A. Truc, A. Quemeneur, P. Hennequin, D. Gresillon, F. Gervais, C. Laviron, J. Olivain, S. K. Saha, and P. Devynck, Rev. Sci. Instrum. **63**, 3716 (1992).
[45]A. Ram, in *11th Top. Conference on Radio Frequency Power in Plasmas, Palm Springs, CA*, edited by R. Prater and V. Chan (American Institute of Physics, New York, 1995) Vol. 355, p. 269.
[46]V. P. Bhatnagar, D. F. H. Start, J. Jacquinot, F. Chaland, A. Cherubini, and F. Porcelli, Nucl. Fusion **12**, 1579 (1994).
[47]F. Porcelli, D. Boucher, and M. N. Rosenbluth, Plasma Phys. Controlled Fusion **38**, 2163 (1996).

Downloaded 11 Apr 2005 to 198.125.178.190. Redistribution subject to AIP license or copyright, see http://pop.aip.org/pop/copyright.jsp